

pubs.acs.org/JPCC Article

Selective Plasmon-Induced Oxidation of 4-Aminothiophenol on **Silver Nanoparticles**

Published as part of The Journal of Physical Chemistry C virtual special issue "Hot Electrons in Catalysis".

Alexander B. C. Mantilla, Bethany E. Matthews, Yi Gu, and Patrick Z. El-Khoury*



Cite This: J. Phys. Chem. C 2023, 127, 8048-8053

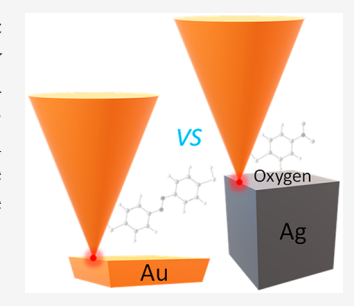


ACCESS

III Metrics & More

Article Recommendations

ABSTRACT: Selectivity in plasmonic chemistry is typically achieved using bimetallic nanostructures. Herein, we show that monometallic silver nanoparticles can also drive highly selective interfacial transformations, oxidation reactions particularly. This is illustrated through a close inspection of tip-enhanced Raman spectral images of 4-aminothiophenol (ATP)functionalized Au vs Ag nanoparticles. We find that whereas the thoroughly described dimerization reaction to form 4,4'-dimercaptoazobenzene dominates the response on Au, highly selective oxidation on Ag nanoparticles exclusively leads to 4-nitrothiophenol. We explore the origin of the distinct reaction pathways on Ag vs Au nanostructures.



■ INTRODUCTION

Exploiting the interactions between plasmonic and molecular systems has enabled significant advances in ultrasensitive chemical detection and imaging. Techniques that rely on the aforementioned interplay between molecules and plasmonic metals, such as surface- and tip-enhanced Raman scattering (SERS¹ and TERS²), have found numerous applications in the physical, biological, and health sciences. Of relevance to our current work are SERS and TERS studies in which plasmoninduced interfacial chemical transformations were tracked with ultrahigh sensitivity (or equivalently spatial resolution) and chemical selectivity.^{3,4} This is possible because the same plasmons that enable enhanced Raman scattering can drive interfacial chemistry as they decay. Using TERS as a probe is particularly lucrative in this context,³ as chemical transformations taking place at solid-air and even solid-liquid interfaces⁵ can be tracked in real space, i.e., with nanometer spatial resolution. Both TERS chemical reaction imaging as well as liquid TERS measurements more broadly were the subjects of recent accounts and review articles.^{3,6} The reader is kindly referred to the recent works for interesting emerging applications and a more detailed exhibition of the current understanding of the underlying physical and chemical phenomena.

Selectivity is often hard to achieve in plasmonic (photo-(electro))chemistry on monometallic nanostructures and nanoparticles.⁷ This is why practitioners have turned to different types of bimetallic structures. Selectivity and reaction yields more generally are difficult to discern using ultrasensitive/high-spatial-resolution TERS. This is in part because of the modified optical selection rules that govern TERS, particularly under ambient laboratory conditions, as discussed in some detail in recent publications from our group.^{8,9} More generally, accounting for concentrations/molecular densities is complicated by the very nature of the TERS response itself, which depends on molecular properties and local fields that vary on the few nanometer length scale in ways that are still not fully understood. For instance, effects such as spatially distinct molecular redox states that can affect the resonance conditions 10 come to mind in this context. In the same vein, spatially varying plasmon resonances have been encountered in the experimental geometry we use herein. 11 These effects and others complicate the analysis of TERS spectral images and hinder quests aimed at quantitative analysis of plasmonassisted chemical processes using this technique.9

Thiophenol derivatives are among the most studied molecular systems in the TERS literature. This is because they easily chemisorb onto plasmonic silver and gold structures and can readily form self-assembled monolayers on metallic surfaces. This is perhaps why in plasmonic photocatalysis, 4nitrothiophenol (NTP) and 4-aminothiophenol (ATP) are the most studied prototypical systems.7 Their dimerization reactions to form 4,4'-dimercaptoazobenzene (DMAB) at solid-air and solid-liquid interfaces have been thoroughly characterized using TERS. 7,12 Different groups have examined

Received: February 21, 2023 Revised: April 11, 2023 Published: April 26, 2023





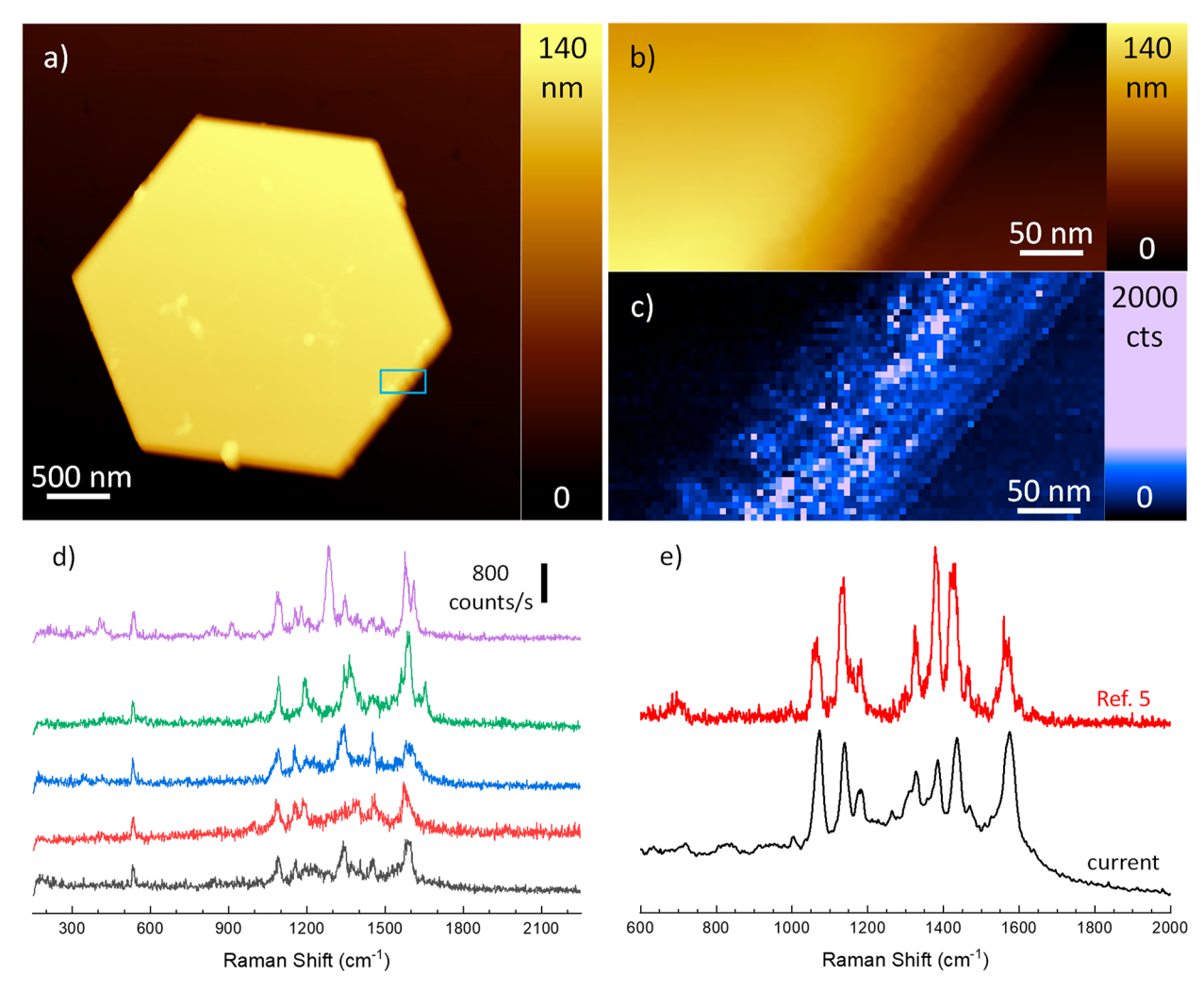


Figure 1. (a) Topographic AFM image of an ATP-coated Au nanoplate. The blue rectangular area highlighted in (a) is further analyzed through simultaneously recorded AFM (b)-TERS (c) mapping. Conditions in (c): $100 \ \mu\text{W}$ @ 633 nm, 1 s time integration, lateral step size = 5 nm. Representative single pixel spectra in (d) show seven peaks in the $1000-1700 \ \text{cm}^{-1}$ spectral region that appear in tandem, albeit featuring variations in peak intensities. Note that these were the brightest spectra in the hyperspectral image cube. Spatial averaging of the bright TERS edge spectra in (c) results in the black spectrum plotted in (e). A previously measured (see Bhattarai et al. 5) TERS spectrum of DMAB is shown on the same plot (red spectrum) in (e) for comparison.

reactions of both NTP and ATP on bimetallic and related monometallic nanostructures. 7,13,14 In the case of NTP, it was found that sandwich-like and alloys of bimetallic structures support reduction reactions to form ATP and DMAB. Such reactions were not observable on related monometallic structures. Similarly, for ATP, a stepwise oxidation reaction was observed that first leads to NTP and then to DMAB. Again, monometallic nanostructures did not support such reaction selectivity. These observations are generally consistent with prior observations and analyses that motivated the adoption of bimetallic nanostructures to achieve product selectivity in plasmonic chemistry.

In this work, we show that reaction selectivity in an oxidation reaction, namely, the plasmon-assisted on-surface synthesis of NTP from ATP, can be achieved using (monometallic) silver nanocubes. Conversely, on Au nanoplates, only DMAB is observed under identical measurement conditions. We deliberate the origin of the herein observed reaction selectivity on Ag vs Au. We find that the most likely explanation for our observations has to do with the higher relative abundance of oxygen on Ag nanocubes compared to

Au nanoplates. We otherwise discuss alternative explanations for our observations, including the roles of molecular orientation and rectified local optical fields. We begin with an overview of the experimental methods used.

METHODS

TERS samples were prepared by depositing silver or gold nanoparticles (Au nanoplates from Nanopartz and Ag nanocubes from Nanocomposix) onto a template stripped gold substrate (PLATYPUS) or a silicon chip, respectively. In both cases, stock solutions of the nanoparticles were used, and a total of 10 μL was drop-casted onto each substrate. The two resulting substrates were then washed using 1 mL of ethanol, followed by drying using N2. Subsequently, 10 μL of a 1 mM ethanolic solution of 4-aminothiophenol (4-ATP, Sigma-Aldrich) was deposited on each sample, followed by rinsing with excess amounts of ethanol. The final samples were dried once more using N2 prior to conducting the TERS measurements.

Our TERS setup is described elsewhere in detail. For this work, as-purchased silicon probes (Nanosensors, ATEC-NC)

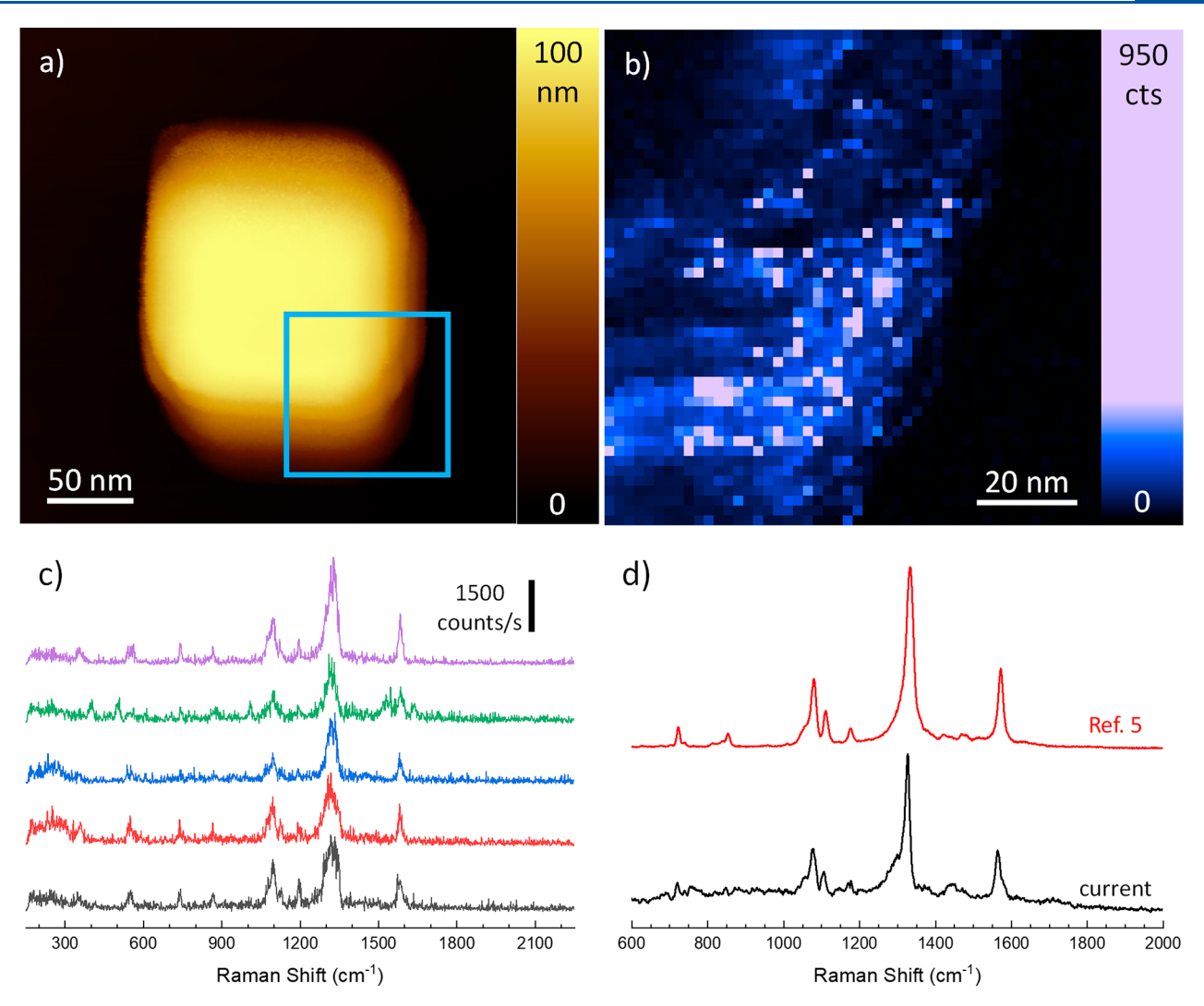


Figure 2. (a) Topographic AFM image of an ATP-coated Ag nanocube. The blue square highlighted in (a) is imaged via TERS in (b). Conditions in (b): $100 \,\mu\text{W}$ @ 633 nm, 0.25 s time integration, lateral step size = 2 nm. Representative single pixel spectra in (c) show three peaks in the $1000-1700 \, \text{cm}^{-1}$ spectral region that appear in tandem, albeit featuring variations in peak intensities. Note that these were the brightest spectra in the hyperspectral image cube. Spatial averaging of the bright TERS edge spectra in (b) results in the black spectrum plotted in (d). A previously measured (see Bhattarai et al. 5) TERS spectrum of NTP is shown on the same plot (red spectrum) in (d) for comparison.

were coated with 100 nm of Au and used for AFM (tapping mode feedback) and TERS (SpecTop, Horiba Scientific) topographical/chemical imaging. For the latter, TERS signals were primarily collected when the tip is in direct contact with the sample. A semicontact mode is otherwise used to move the sample relative to the tip (pixel to pixel). Additional TERS spectral images were collected for the Ag nanocubes using a tapping mode AFM feedback, as described in a previous work from our group. 15 For all TERS measurements, a 633 nm diode laser (75-100 μ W) was focused onto the tip apex at a \sim 65° angle with respect to the surface normal using a 100× air objective (Mitutoyo, 0.7 NA). The polarization of the laser was set to coincide with the tip long axis using a half-waveplate. The backscattered light was collected using the same objective, filtered through a series of long pass/dichroic filters, and recorded using a CCD camera (Andor, Newton EMCCD) coupled to a spectrometer (Andor, Kymera 328i) equipped with a 600 line/mm grating blazed at 550 nm.

STEM high-angle annular dark field (STEM-HAADF) images were collected on a probe-corrected JEOL ARM-200CF microscope operating at 200 kV, with a 1 Å probe size,

a 27.5 mrad convergence semiangle, and a 68 mrad collection semiangle. STEM energy-dispersive X-ray spectroscopy (STEM-EDS) maps were acquired using a JEOL Centurio silicon drift detector with a combined solid collection angle of 0.98 sr. The maps shown were processed for the Ag-L, Au-L, and O-K peaks.

RESULTS AND DISCUSSION

Our first sets of measurements track a familiar reaction, namely, the dimerization of ATP to form DMAB. The results are summarized in Figure 1. We started by identifying an ATP-functionalized gold nanoplate using topographic AFM imaging. With prior TERS demonstrations in mind, we expected the signal to be optimally enhanced toward the edges of the plate under our experimental conditions. We therefore focus our analysis to the small rectangular area highlighted in Figure 1a. Simultaneously recorded AFM-TERS (panels b and c, respectively) maps of this area reveal that the signal is indeed optimal toward the edge of the Au structure. Not surprisingly, we find that the TERS spectra are dominated by the signatures of DMAB. Although the relative intensities of the DMAB

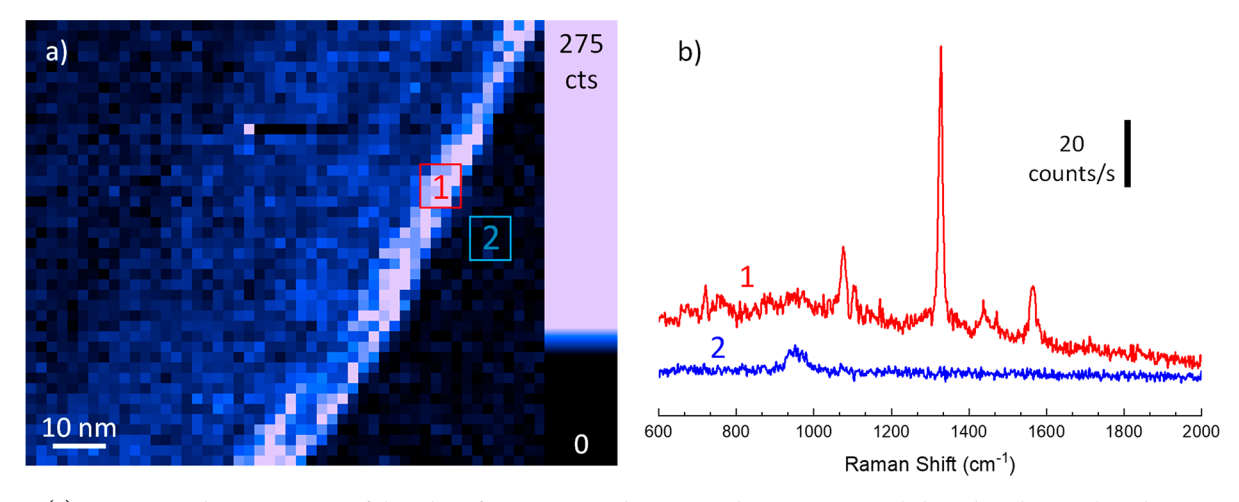


Figure 3. (a) Tapping mode TERS image of the edge of an ATP-coated Ag nanocube. Spectra recorded on the edge vs when the tip was a few nanometers away from the cube are shown on the same plot in (b). These plots were recorded at the locations indicated using squares in (a). Conditions: 100 μ W @ 633 nm, 0.5 s time integration, lateral step size = 2 nm.

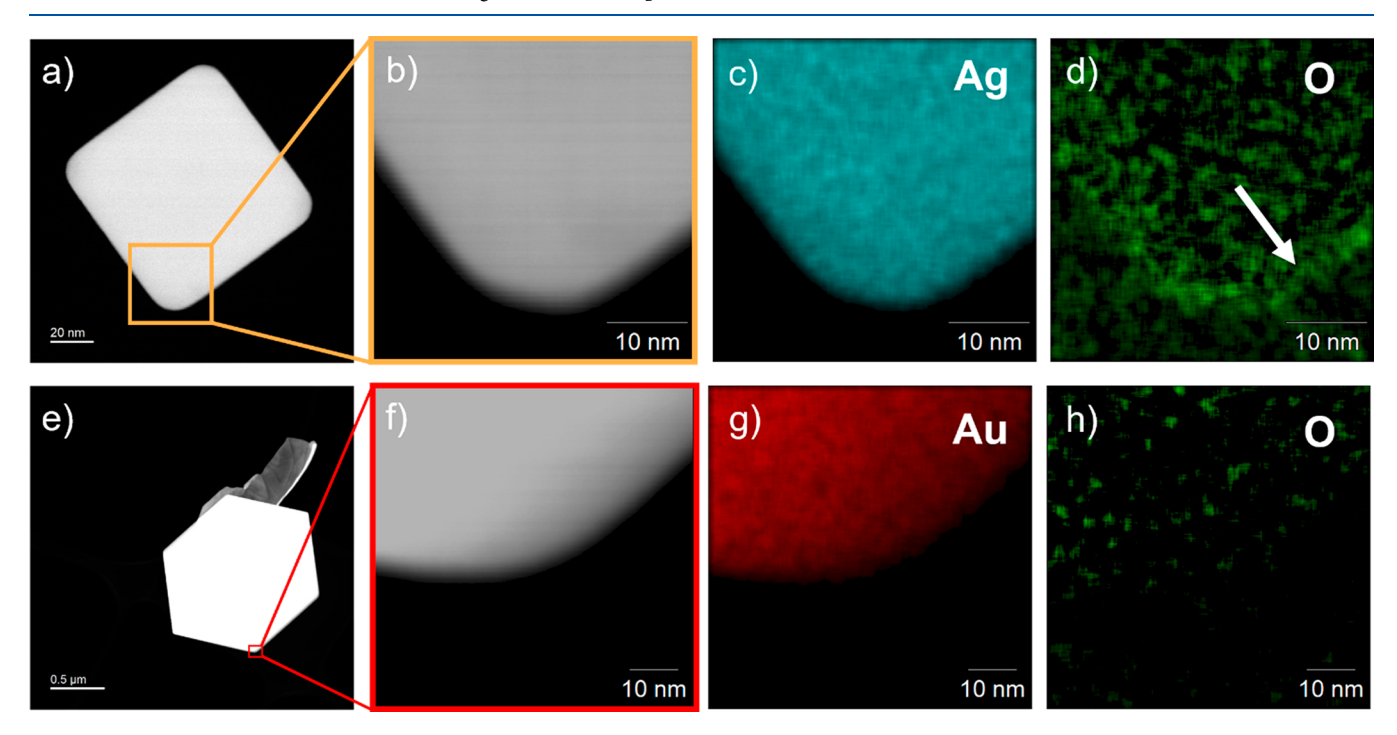


Figure 4. STEM HAADF images of a Ag nanocube (a,b) viewed side-on and of a Au nanoplate (e,f). STEM-EDS mapping (c,d) of Ag-L and O-K from (b) shows the surface of the Ag is oxidized, as highlighted by the white arrow in (d). STEM-EDS maps of Au-L and O-K (g,h) from (f) show no O-K signal toward the edge of the nanoplate.

TERS spectra vary across the edge (panel d), the peaks all appear in tandem and mark the formation of the dimer product. Spatial averaging of the edge response and its comparison with a previously recorded DMAB TERS spectrum⁵ adds confidence to our assignment. The reader is referred to prior work for theoretical analyses of the DMAB spectrum and spectral assignments.¹⁶

Repeating the same measurements and analysis described above but now using an ATP-functionalized Ag nanocube results in distinct observations. The results of these measurements are summarized in Figure 2. In this case, the edge spectra again reveal distinct relative intensities of the observable vibrational resonances (Figure 2c) that can be assigned to NTP on the basis of previous work. Here and above (Figure 1), the relative intensity differences at different

sites can be associated with distinct orientations of molecules relative to vector components of the local optical fields. These effects become noticeable in high-spatial-resolution measurements, herein pixel-limited to within 2 nm. The latter, which can be inferred from the image shown in Figure 2b, is consistent with several prior measurements from our group that targeted chemically functionalized silver nanocubes. Sp. In Figure 2d, the spatially averaged TERS response at the edge that is visualized in Figure 2b is compared to a previously reported and carefully assigned TERS spectrum of NTP. Beyond a good general agreement between the herein and previously recorded spectra, it is important to note that the ~1335 cm⁻¹ resonance of NTP is asymmetric in both cases. Indeed, a broad shoulder that arises from a distinct resonance centered at ~1290 cm⁻¹ is observed. This marks the formation

of anionic NTP species,¹⁷ and it is particularly evident in the lower black spectrum in Figure 2d.

The formation of anionic NTP species can be suppressed by switching from (intermittent) contact (Figures 1 and 2) to tapping mode AFM feedback in TERS, as discussed in a prior work. 15 Moving away from contact also suppresses optical field rectification in the TERS geometry, which has been recently implicated with plasmonic chemistry on bimetallic nanostructures. 18 To this end, we repeated the measurements shown in Figure 2b but now using tapping mode AFM feedback. The results are summarized in Figure 3, and they reveal that the optical signature of NTP once again dominates the TERS response. Consistent with prior observations, the symmetric NO₂ stretching vibration in Figure 3b indicates that molecular charging is now suppressed. The observations are otherwise identical to their analogues in Figure 2. Evidently, it appears that neither the formation of anions nor rectified local optical fields plays a role in the observed oxidation (on Ag) vs dimerization (on Au) reactions described above. The fact that different resonances are accessible with the 633 nm excitation wavelength in contact vs tapping mode TERS¹⁵ and the spatially varying nature of junction plasmon resonances in TERS¹¹ both suggest that spatially varying resonances cannot exclusively account for our observations.

The different chemical reaction pathways that lead to distinct products on Au vs Ag nanostructures may be rationalized on the basis of the results that are summarized in Figure 4. In this plot, we visualize the relative abundance of oxygen at the surfaces (edges in the TEM geometry) of the two structures used in this work. Two particles atop a laceycarbon Cu TEM grid were examined by STEM-HAADF imaging (a,b,e,f) and STEM-EDS analysis (c,d,g,h). The upper panels analyze the Ag nanoparticle along its (001) zone, while the lower panels are corresponding morphological and elemental composition images of a Au nanoplate. The differences in surface oxygen content in the two cases can be immediately discerned by comparing Figures 4d (Ag) and 4h (Au). Indeed, the bright oxygen signal observed in Figure 4d, which outlines the edges of the nanocube, is not observed in the case of the gold structure.

There are two possible explanations for the observed distinct reaction channels and products on Au vs Ag structures. In the first scenario, one can argue that the local availability of a reactant (oxygen) leads to the oxidation of ATP to form NTP. In the second case, the surface oxygens play a secondary role by leading to distinct adsorption geometries of ATP on Ag. Molecular orientation was recently invoked in rationalizing the lack of the coupling/dimerization reaction for both ATP and NTP on $Ag(111)^{19}$ Interestingly, the relative intensities of the observable vibrational states in TERS were very similar on Ag(111) and Au(111) in the previous work, 19 which to us suggests that the orientations on both surfaces were similar. Nonetheless, theoretical analyses in the prior work suggested otherwise.¹⁹ Orientations cannot be checked in our current study, e.g., using previously outlined procedures,9 since we do not observe ATP but rather products directly under our experimental conditions. That said, it is certainly possible for the few nm thick oxide layer that we observe in Figure 4d to alter the orientation of ATP near the surface. Direct chemisorption on Au otherwise leads to a geometry/ conformation that favors dimerization to form DMAB. More work is needed to systematically distinguish between the two above-outlined possibilities.

CONCLUSIONS

In conclusion, this work demonstrates that distinct plasmon-induced chemical transformations take place on Au and Ag nanostructures that are functionalized with ATP. Our results suggest that the abundance of surface oxygen either directly or indirectly leads to oxidation to form NTP on Ag. Direct chemisorption onto Au nanoplates otherwise leads to DMAB, which is consistent with several prior reports from our group and others. How oxidation and distinct conformations at the surfaces of plasmonic metals affect local chemical reactivity remains an open question in plasmonic photocatalysis and heterogeneous catalysis more generally. This motivates further studies to understand how orientations and conformations alter the ground and excited state properties of molecules that dynamically interact with metals, particularly under ambient laboratory conditions.

AUTHOR INFORMATION

Corresponding Author

Patrick Z. El-Khoury — Physical Sciences Division, Pacific Northwest National Laboratory, Richland, Washington 99352, United States; orcid.org/0000-0002-6032-9006; Email: patrick.elkhoury@pnnl.gov

Authors

Alexander B. C. Mantilla – Department of Physics and Astronomy, Washington State University, Pullman, Washington 99164, United States; orcid.org/0000-0002-9262-1351

Bethany E. Matthews — Energy and Environment Directorate, Pacific Northwest National Laboratory, Richland, Washington 99352, United States; orcid.org/0000-0001-7193-2583

Yi Gu — Department of Physics and Astronomy, Washington State University, Pullman, Washington 99164, United States

Complete contact information is available at: https://pubs.acs.org/10.1021/acs.jpcc.3c01204

Notes

The authors declare the following competing financial interest(s): YG has equity interest in Klar Scientific.

ACKNOWLEDGMENTS

ABCM and YG acknowledge support from the National Science Foundation (DMR-2004655). PZE acknowledges support from the U.S. Department of Energy, Office of Science, Basic Energy Sciences, Chemical Sciences, Geosciences, and Biosciences Division, Condensed Phase and Interfacial Molecular Science program, FWP 16248. Part of the instrumentation that was required to perform the measurements described herein were purchased and developed as part of a PNNL LDRD project (under the chemical dynamics initiative). The latter project (PNNL LDRD) also supported the TEM measurements and their analysis.

REFERENCES

(1) Zrimsek, A. B.; Chiang, N. H.; Mattei, M.; Zaleski, S.; McAnally, M. O.; Chapman, C. T.; Henry, A. I.; Schatz, G. C.; Van Duyne, R. P. Single-Molecule Chemistry with Surface- and Tip-Enhanced Raman Spectroscopy. *Chem. Rev.* **2017**, *117*, 7583–7613.

(2) Cao, Y.; Sun, M. Tip-Enhanced Raman Spectroscopy. Rev. Phys. 2022, 8, 100067.

- (3) Li, Z. D.; Kurouski, D. Plasmon-Driven Chemistry on Monoand Bimetallic Nanostructures. Acc. Chem. Res. 2021, 54, 2477-2487.
- (4) Warkentin, C. L.; Yu, Z.; Sarkar, A.; Frontiera, R. R. Decoding Chemical and Physical Processes Driving Plasmonic Photocatalysis using Surface-Enhanced Raman Spectroscopies. Acc. Chem. Res. 2021, 54, 2457-2466.
- (5) Bhattarai, A.; El-Khoury, P. Z. Nanoscale Chemical Reaction Imaging at the Solid-Liquid Interface via TERS. J. Phys. Chem. Lett. 2019, 10, 2817.
- (6) Britz-Grell, A. B.; Saumer, M.; Tarasov, A. Challenges and Opportunities of Tip-Enhanced Raman Spectroscopy in Liquids. J. Phys. Chem. C 2021, 125, 21321-21340.
- (7) Quiroz, J.; Barbosa, E. C. M.; Araujo, T. P.; Fiorio, J. L.; Wang, Y.-C.; Zou, Y.-C.; Mou, T.; Alves, T. V.; de Oliveira, D. C.; Wang, B.; et al. Controlling Reaction Selectivity over Hybrid Plasmonic Nanocatalysts. Nano Lett. 2018, 18, 7289-7297.
- (8) El-Khoury, P. Z.; Schultz, Z. D. From SERS to TERS and Beyond: Molecules as Probes of Nanoscopic Optical Fields. J. Phys. Chem. C 2020, 124, 27267-27275.
- (9) El-Khoury, P. Z. Tip-Enhanced Raman Scattering on Both Sides of the Schrödinger Equation. Acc. Chem. Res. 2021, 54, 4576-4583.
- (10) Sloan-Dennison, S.; Zoltowski, C. M.; El-Khoury, P. Z.; Schultz, Z. D. Surface Enhanced Raman Scattering Selectivity in Proteins Arises from Electron Capture and Resonant Enhancement of Radical Species. J. Phys. Chem. C 2020, 124, 9548-9558.
- (11) Wang, C.-F.; El-Khoury, P. Z. Multimodal Tip-Enhanced Nonlinear Optical Nanoimaging of Plasmonic Silver Nanocubes. J. Phys. Chem. Lett. 2021, 12, 10761-10765.
- (12) Van Schrojenstein Lantman, E. M.; Deckert-Gaudig, T.; Mank, A. J. G.; Deckert, V.; Weckhuysen, B. M. Catalytic Processes Monitored at the Nanoscale with Tip-Enhanced Raman Spectroscopy. Nat. Nanotechnol. 2012, 7, 583-586.
- (13) Fang, Y.; Li, Y.; Xu, H.; Sun, M. Ascertaining P,P'-Dimercaptoazobenzene Produced from P-Aminothiophenol by Selective Catalytic Coupling Reaction on Silver Nanoparticles. Langmuir 2010, 26, 7737-7746.
- (14) Lin, W.; Cao, E.; Zhang, L.; Xu, X.; Song, Y.; Liang, W.; Sun, M. Electrically Enhanced Hot Hole Driven Oxidation Catalysis at the Interface of a Plasmon-Exciton Hybrid. Nanoscale 2018, 10, 5482-5488.
- (15) Wang, C. F.; O'Callahan, B. T.; Kurouski, D.; Krayev, A.; Schultz, Z. D.; El-Khoury, P. Z. Suppressing Molecular Charging, Nanochemistry, and Optical Rectification in the Tip-Enhanced Raman Geometry. J. Phys. Chem. Lett. 2020, 11, 5890-5895.
- (16) Aprà, E.; Bhattarai, A.; Baxter, E.; Wang, S.; Johnson, G. E.; Govind, N.; El-Khoury, P. Z. Simplified Ab Initio Molecular Dynamics-Based Raman Spectral Simulations. Appl. Spectrosc. 2020, 74, 1350.
- (17) Wang, C. F.; O'Callahan, B. T.; Kurouski, D.; Krayev, A.; ElKhoury, P. Z. The Prevalence of Anions at Plasmonic Nanojunctions: A Closer Look at p-Nitrothiophenol. J. Phys. Chem. Lett. **2020**, 11, 3809-3814.
- (18) Li, Z.; Rigor, J.; Large, N.; El-Khoury, P.; Kurouski, D. Underlying Mechanisms of Hot Carrier-Driven Reactivity on Bimetallic Nanostructures. J. Phys. Chem. C 2021, 125, 2492-2501.
- (19) Sun, J.-J.; Su, H.-S.; Yue, H.-L.; Huang, S.-C.; Huang, T.-X.; Hu, S.; Sartin, M. M.; Cheng, J.; Ren, B. Role of Adsorption Orientation in Surface Plasmon-Driven Coupling Reactions Studied by Tip-Enhanced Raman Spectroscopy. J. Phys. Chem. Lett. 2019, 10, 2306.

□ Recommended by ACS

Near Field Scattering Optical Model-Based Catalyst Design for Artificial Photoredox Transformation

Ming-Yu Qi, Yi-Jun Xu, et al.

MARCH 08, 2023

ACS CATALYSIS

READ 2

Mechanistic Insights into Plasmonic Catalysis by Dynamic Calculations: O₂ and N₂ on Au and Ag Nanoparticles

Connor J. Herring and Matthew M. Montemore

FEBRUARY 13, 2023

CHEMISTRY OF MATERIALS

READ **C**

Elucidating the Roles of Local and Nonlocal Rate Enhancement Mechanisms in Plasmonic Catalysis

Rachel C. Elias and Suljo Linic

OCTOBER 24, 2022

JOURNAL OF THE AMERICAN CHEMICAL SOCIETY

READ **C**

Trimetallic Nanostructures of Silver-Platinum Alloy Shells on Gold Nanorods for Plasmon-Mediated Photocatalysis

Qi Zhang, Zhiqun Cheng, et al.

NOVEMBER 09, 2022

ACS APPLIED NANO MATERIALS

READ 2

Get More Suggestions >